IOPscience iopscience.iop.org

Home Search Collections Journals About Contact us My IOPscience

Tunneling of Dirac electrons through one-dimensional potentials in graphene: a *T*-matrix approach

This article has been downloaded from IOPscience. Please scroll down to see the full text article.

2009 J. Phys.: Condens. Matter 21 045305

(http://iopscience.iop.org/0953-8984/21/4/045305)

View the table of contents for this issue, or go to the journal homepage for more

Download details:
IP Address: 129.252.86.83
The article was downloaded on 29/05/2010 at 17:28

Please note that terms and conditions apply.

J. Phys.: Condens. Matter **21** (2009) 045305 (6pp) doi:10.1088/0953-8984/21/4/045305

Tunneling of Dirac electrons through one-dimensional potentials in graphene: a T-matrix approach

H Chau Nguyen and V Lien Nguyen[1]

Theoretical Department, Institute of Physics, VAST, PO Box 429 Bo Ho, Hanoi 10000, Vietnam

E-mail: nvlien@iop.vast.ac.vn

Received 13 October 2008
Published 8 January 2009
Online at stacks.iop.org/JPhysCM/21/045305

Abstract

The standard T-matrix method can be effectively used for studying the dynamics of Dirac electrons under one-dimensional potentials in graphene. The transmission probability expressed in terms of T-matrices and the corresponding ballistic current are derived for any smooth one-dimensional potential, taking into account the chirality of Dirac massless carriers. Numerical calculations are illustrated for the potential approximately describing graphene n–p junctions.

While conventional two-dimensional (2D) electron gases are practically formed by confining electrons in MOSFETs or semiconductor heterostructures, graphene is a truly two-dimensional crystal. As the limiting variance of carbon nanotubes, graphene is a single layer of carbon atoms densely packed in a honeycomb lattice which can be treated as two interpenetrating triangular sublattices often labeled A and B. The most important consequence of such a crystal structure is the linear dispersion relation with electron–hole symmetry near the charge neutrality points in the energy band structure, $|E| = \hbar v_{\mathrm{F}}|\delta k|$, where $v_{\mathrm{F}} \approx 10^6$ m s^{-1} is the Fermi velocity and $\delta\mathbf{k} = \mathbf{k} - \mathbf{K}$ is the displacement of the wavevector $\mathbf{k}$ from the neutrality point $\mathbf{K}$ [1–4]. So, the low energy excitations in graphene are massless fermions which have been shown to exhibit potentially useful properties such as a remarkably high mobility, even at room temperature, or weak spin–orbit and hyperfine couplings (see [2] and references therein). Surprisingly, even though v_{F} is very small compared to the speed of light, the dynamics of these low energy excitations seems to be governed by the 2D Dirac relativistic equation [5, 6]:

$$[v_{\mathrm{F}}(\vec{\sigma}\,\hat{p}) + U(x)]\Psi = E\Psi, \tag{1}$$

where the pseudospin matrix $\vec{\sigma}$ has components given by the Pauli matrices, $\hat{p} = (p_x, p_y)$ is the in-plane momentum operator, and U is a potential which is in this work assumed to be one-dimensional (1D), $U \equiv U(x)$. 1D-potential problems are always interesting from the point of view of both fundamentals and practical applications. In such a potential the eigenstates Ψ of the equation (1) have the form $\Psi = \Phi(x)\exp(\mathrm{i}k_y y)$, where k_y is the transverse wavenumber and $\Phi(x)$ are two-component spinors, $\Phi = [\varphi_{\mathrm{A}}, \varphi_{\mathrm{B}}]^{\mathrm{T}}$ with $\Psi_A = \varphi_{\mathrm{A}}\exp(\mathrm{i}k_y y)$ and $\Psi_{\mathrm{B}} = \varphi_{\mathrm{B}}\exp(\mathrm{i}k_y y)$ being the envelope functions associated with the probability at the respective sublattice sites A and B of the graphene sheet. The equation (1) then reduces to following equations for φ_{A} and φ_{B}:

$$\begin{aligned} -\mathrm{i}\hbar v_{\mathrm{F}}\left(\frac{\partial}{\partial x} + k_y\right)\varphi_{\mathrm{B}} + (U(x) - E)\varphi_{\mathrm{A}} = 0, \\ -\mathrm{i}\hbar v_{\mathrm{F}}\left(\frac{\partial}{\partial x} - k_y\right)\varphi_{\mathrm{A}} + (U(x) - E)\varphi_{\mathrm{B}} = 0. \end{aligned} \tag{2}$$

Unfortunately, even for relatively simple forms of $U(x)$ these equations (2) cannot always be analytically solved. Different approximations and/or numerical calculations need to be used, depending on the form of $U(x)$ (see, for example, [7–9]).

In this work we show that the transfer (T) matrix method, well known in low-dimensional semiconductor physics [10], can be used as an effective approach for solving equation (2) with any smooth potential $U(x)$. The advantage of T-matrices is that they can easily be multiplied to build up complicated potentials in one dimension. Indeed, let us consider a potential $U(x)$ as schematically illustrated in figure 1(a). The region

[1] Author to whom any correspondence should be addressed.

 © 2009 IOP Publishing Ltd Printed in the UK

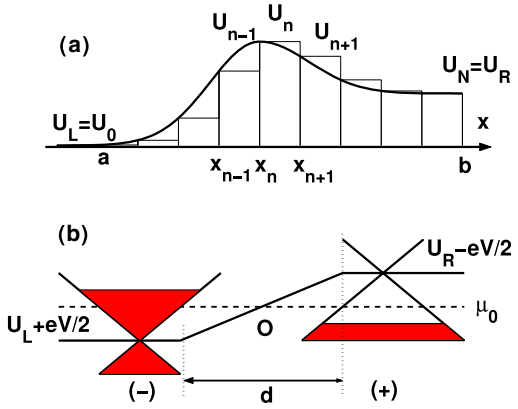

Figure 1. (a) Illustration of how the T-matrix can be constructed for a smooth 1D-potential $U(x)$ with the active region (a, b) ($U_{\rm L}(U_{\rm R})$ is the potential in the left (right) lead). (b) The potential (9) approximately models a graphene n–p junction. The case of forward biases is demonstrated.

(This figure is in colour only in the electronic version)

where U varies with x will be called an active region (see region (a, b) in figure 1(a)). Beyond this region, $U(x) \equiv U_{\rm L} = \text{const}$ in the left lead and $U(x) \equiv U_{\rm R} = \text{const}$ in the right one (see regions $x < a$ and $x > b$, respectively, in figure 1(a)). So, we will be interested in the tunneling of Dirac electrons from the left lead to the right one through the active potential region. For any smooth potential, in principle, this region can be approximately treated as a series of many steep potentials so that within each step the potential can be considered constant. The overall T-matrix to be found is then simply given by multiplying the partial T-matrices for all the steep potentials. On the other hand, for each steep potential the partial T-matrix can be obtained from the solutions of equation (2) in the left and the right side of it (where the potential U is constant) by requiring an appropriate condition of continuity at the steep interface. The calculating procedure is the same as in semiconductor structures, but the continuity is only required here for wavefunctions (by matching up the corresponding amplitudes).

Let us consider, for example, the nth-step defined by $x_n < x < x_{n+1}$, $(n = 0, 1, 2, \ldots, N-1$, where $x_0 \equiv a$ and $x_N \equiv b)$. Within this step $U(x) \approx U_n = \text{const}$ and solutions of equation (2) have the general form:

$$\varphi_{\rm A}(x) = A_n e^{ik_n x} + B_n e^{-ik_n x},$$

$$\varphi_{\rm B}(x) = \frac{\hbar v_{\rm F}}{E - U_n}[(k_n + ik_y)A_n e^{ik_n x} - (k_n - ik_y)B_n e^{-ik_n x}], \tag{3}$$

where $k_n = \sqrt{[(E-U_n)/\hbar v_{\rm F}]^2 - k_y^2}$. Equations (3) can for convenience be rewritten in the matrix form

$$\begin{pmatrix} \varphi_{\rm A}(x) \\ \varphi_{\rm B}(x) \end{pmatrix} = \mathbf{M}_n * \mathbf{R}_n(x) * \begin{pmatrix} A_n \\ B_n \end{pmatrix}. \tag{4}$$

Here the two auxiliary matrices $\mathbf{M}_n$ and $\mathbf{R}_n$ are defined as

$$\mathbf{M}_n = \begin{pmatrix} 1 & 1 \\ \frac{\hbar v_{\rm F}(k_n + ik_y)}{E - U_n} & -\frac{\hbar v_{\rm F}(k_n - ik_y)}{E - U_n} \end{pmatrix} \quad \text{and}$$

$$\mathbf{R}_n = \begin{pmatrix} e^{ik_n x} & 0 \\ 0 & e^{-ik_n x} \end{pmatrix}. \tag{5}$$

Using these matrices and $\mathbf{C}_n \equiv (A_n, B_n)^{\rm T}$, the condition of continuity of wavefunctions at the interface, located at $x = x_n$, between the $(n-1)$- and n-steps takes a very compact form: $\mathbf{M}_{n-1}\mathbf{R}_{n-1}(x_n)\mathbf{C}_{n-1} = \mathbf{M}_n\mathbf{R}_n(x_n)\mathbf{C}_n$, which yields $\mathbf{C}_n = \mathbf{R}_n^{-1}(x_n)\mathbf{M}_n^{-1}\mathbf{M}_{n-1}\mathbf{R}_{n-1}(x_n)\mathbf{C}_{n-1}$. Hence, by definition, the partial T-matrix between the two indicated steps can be straightforwardly obtained: $\mathbf{T}(n, n-1) = \mathbf{R}_n^{-1}(x_n)\mathbf{M}_n^{-1}\mathbf{M}_{n-1}\mathbf{R}_{n-1}(x_n)$. Further, the overall T-matrix for the whole 1D-potential, approximated by a series of N steps between a and b, is simply the product:

$$\mathbf{T} \equiv \mathbf{T}(N, 0) = \mathbf{T}(N, N-1) * \mathbf{T}(N-1, N-2) * \cdots * \mathbf{T}(1, 0).$$

In practice, such a procedure of constructing the overall T-matrix can be easily realized computationally without the need to write down intermediate wavefunctions.

From the T-matrix, as a rule, one can directly deduce the transmission probability $\mathcal{T}$. For graphene, however, it is important to notice that both electrons (with positive energies) and holes (with negative energies) can simultaneously contribute to the transmission probability at the Fermi level. Taking into account this specific property, as shown in the appendix, we can derive the following expression for the transmission probability of the state (E, α) from the left ($x < a$ where $U(x) \equiv U_{\rm L}$) to the right ($x > b$ where $U \equiv U_{\rm R}$) of the active region:

$$\mathcal{T}(E, \alpha) = f(s, \alpha) \begin{cases} 1 - |T_{21}|^2/|T_{22}|^2 & \text{if } (E - U_{\rm L}) \text{ and} \\ \qquad (E - U_{\rm R}) \text{ have the same sgn} \\ 1 - |T_{22}|^2/|T_{21}|^2 & \text{otherwise} \end{cases} \tag{6}$$

where the meaning of all symbols is given in the appendix. This expression of $\mathcal{T}$ is rather general and can be used for any smooth potential $U(x)$. In the presence of an applied bias voltage, despite the change of potential profile, making all the step-potentials $U_n (n = 0, 1, \ldots, N)$ depending on the bias, the procedure of constructing the overall T-matrix remains the same as in the case without bias and the expression (6) gives $\mathcal{T}$ as a function of bias.

Further, in a way similar to that discussed in detail in [11], the zero-temperature ballistic current can be easily derived:

$$I = \frac{2geW}{v_{\rm F}h^2}\int_{\mu_{\rm R}}^{\mu_{\rm L}} {\rm d}E\,|E - U_{\rm L}| \times \int_{-\pi}^{\pi} {\rm d}\alpha\,\text{sgn}(E - U_{\rm L})\mathcal{T}(E, \alpha)\cos\alpha, \tag{7}$$

where e is the elementary charge, $g = 4$ is the degeneracy of electron states in graphene, W is the sample width, which is assumed to be large so that the edge effects can be neglected [12], and $\mu_{\rm L}(\mu_{\rm R})$ is the bias-dependent local Fermi energy in the left (right) lead. The applied voltage V is defined as $eV = \mu_{\rm L} - \mu_{\rm R}$ for forward-biased junctions or $eV = \mu_{\rm R} - \mu_{\rm L}$ for reverse-biased junctions. So, the expression (7)

describes the current–voltage (I–V) characteristics which in the linear regime provide the conductance:

$$G = \frac{2ge^2W}{v_F h^2}|\mu_0 - U_L| \int_{-\pi}^{\pi} d\alpha \, \mathrm{sgn}(\mu_0 - U_L)\mathcal{T}(\mu_0, \alpha)\cos\alpha, \tag{8}$$

where μ_0 is the equilibrium Fermi energy, $\mu_0 = \mu_L(0) = \mu_R(0)$. Notice that the product $\mathrm{sgn}(E - U_L)\mathcal{T}(E, \alpha)\cos\alpha$ under the integral in equation (7) (or $\mathrm{sgn}(\mu_0 - U_L)\mathcal{T}(\mu_0, \alpha)\cos\alpha$ in equation (8)) is always positive and that both U_L and U_R in equation (7) are bias dependent. The expressions (7) and (8) are rather general and can be used for any smooth 1D-potential.

As an illustration for the approach suggested, we consider the potential (figure 1(b)):

$$U(x) = \begin{cases} U_L & \text{for } x \leqslant a \\ U_L + [(x-a)/(b-a)](U_R - U_L) & \\ \qquad \text{for } a < x < b & \\ U_R & \text{for } x \geqslant b. \end{cases} \tag{9}$$

This potential, though very simple, is the classical model for studying so-called Klein tunneling [13] and, moreover, it also approximately describes the graphene n–p junctions [8, 14, 15]. The potential (9) is in fact characterized by the two parameters of barrier height $\Delta U = (U_R - U_L)$ and junction width $d = (b - a)$. However, since the qualitative tunneling feature of the studied junction is essentially determined by only the 'field' $\Delta U/d$ [7, 8], it is reasonable to examine those potentials with different d, keeping ΔU constant. Moreover, we can always for convenience choose the origin of potential so that in the absence of bias $U_R = -U_L > 0$, making the potential symmetric (with respect to the point O in figure 1(b)). Thus, given $\Delta U \equiv 2U_R$, we can calculate the transmission probability $\mathcal{T}$ (6) as a function of E and α, and then the current (7) and the conductance (8) for the junctions (9) with different d. The obtained results are presented in figures 2–5, where ΔU is uniquely set to be 60 meV and our discussion will be about the well addressed incident angle β [4, 8] rather than the angle α in equation (6) (see the appendix for the relation between these two angles).

In figure 2 the transmission probability $\mathcal{T}$ is displayed as a function of the incident energy E for three junctions with different d: 0 (solid), 60 nm (dashed) and 120 nm (dash-dotted line), given the incident angle $\beta = \pi/9$. The most impressive feature of these curves is that observed in the low energy region, where unlike conventional semiconductor junctions $\mathcal{T}$ is non-zero, or even reaches its maximum value of unity (depending on the incident angle β). Consequently, in $\mathcal{T}(E)$-curves there may exist a hard well with zero-$\mathcal{T}$ inside. Such a well is associated with evanescent waves in the right lead and appears in the energy range $U_L + \Delta U/(1 + |\sin\beta|) < E < U_L + \Delta U/(1 - |\sin\beta|)$. The well width is then proportional to ΔU and depends on the incident angle β as $\Delta E_g = 2\Delta U|\sin\beta|/(1+\sin^2\beta)$. For normal incident carriers, $\beta = 0$, the well disappears and the potential is perfectly transparent ($\mathcal{T} = 1$) in agreement with the Klein tunneling concept of massless particles (the dotted line in the top of this figure, see also the next figure). On the other hand, though

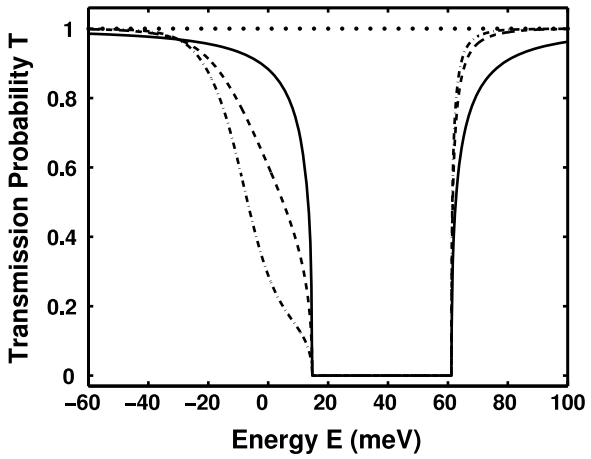

Figure 2. Transmission probability $\mathcal{T}$ as a function of the incident energy E for three potentials with the same $\Delta U = 60$ meV, but with different d: 0 (solid), 60 nm (dashed), and 120 nm (dash-dotted line). The angle of incidence $\beta = \pi/9$. The dotted line at the top shows the case $\beta = 0$ when the potential is perfectly transparent.

the well ΔE_g is independent of the junction width d, the transmission $\mathcal{T}$ in the Klein tunneling region, $U_L < E < U_L + \Delta U/(1 + |\sin\beta|)$, considerably decreases as d increases (compare the three curves with different d in the energy range -30 meV $< E <$ 15 meV in figure 2). This is again in agreement with the Klein tunneling concept [4, 8, 13]. On the contrary, a slight increase of $\mathcal{T}$ with d in the regions of lower ($E < U_L$) and higher energies ($E \geqslant U_L + (U_R - U_L)/(1 - |\sin\beta|)$) is the familiar character of conventional electron (hole) tunneling through the considered 1D-potential (see, for example, [16]).

Figure 3 shows the dependence on angle of incidence of $\mathcal{T}$ for the junction with $d = 60$ nm and with different energies E: (1) -60 meV $< U_L$ (2) 0 (in the Klein tunneling region), and (3) 60 meV $> U_R$. Clearly, due to Klein tunneling [4, 13] the potential is always perfectly transparent ($\mathcal{T} = 1$) for angles β close to the normal incidence $\beta = 0$, regardless of incident energy E. An increase in $|\beta|$ causes an enhancement of the magnitude of the transverse wavenumber, $|k_y| = (|E - U_L|/\hbar v_F)|\sin\beta|$, that in turn leads to a reduction of $\mathcal{T}$ [4, 8, 9]. The features of such a $\mathcal{T}$-reduction depend on $|k_y|$, i.e. on the incident energy E, as can be seen in this figure. For $E < U_L$ (curve (1)) the transparency of the studied potential is mainly associated with the tunneling of the holes through a downward potential. In this case the transmission probability $\mathcal{T}$ is non-zero for any β in the range $-\pi/2 < \beta < \pi/2$. On the contrary, for $E > U_L$, when the tunneling of electrons through an upward potential is dominant (curve (3) for $E > R_R$) or when the Klein tunneling plays an essential role (curve (2) for $U_L < E < U_R$), the transmission $\mathcal{T}$ is non-zero only in a narrow range of incident angles β defined by $|\sin\beta| < |E - U_R|/|E - U_L|$. In particular, in the case of $U_L < E < U_R$, the transmission probability for the considered potential has been semiclassically derived [8]:

$$\mathcal{T} = \exp(-\pi v_F k_y^2 d/\Delta U). \tag{10}$$

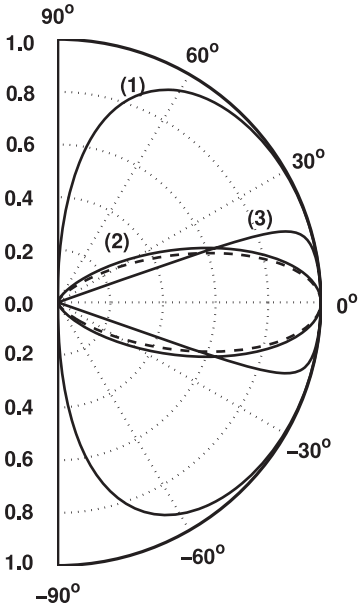

Figure 3. Incident angle dependence of $\mathcal{T}$: three solid curves are calculated from equation (6) for the same potential of $\Delta U = 60$ meV and $d = 60$ nm, but with different incident energies E: (1) −60, (2) 0, and (3) 60 meV. The dashed line displays expression (8) in comparison with the solid curve (2).

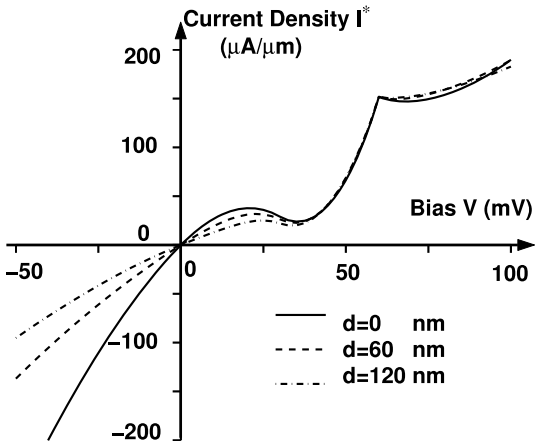

Figure 4. I–V characteristics $I^*(V)$ for three junctions with the same ΔU but with different d from those studied in figure 2 in the forward bias ($V > 0$) and the reverse bias regime ($V < 0$): $d = 0$ (solid), 60 nm (dashed), and 120 nm (dash-dotted line).

This expression for $\mathcal{T}$ is displayed in figure 3 by the dashed curve for the same junction parameters and the same energy E as those for the solid curve (2). There is clearly a good agreement between the solid curve (2) calculated from equation (6) and the dashed curve deduced from expression (10). Notice, however, that the expression (10) has been derived for only the energies in the Klein tunneling region [18], so it cannot describe, for example, the solid curves (1) [$E < U_L$] and (3) [$E > U_R$] in figure 3. Notice also that although $\mathcal{T}$ depends on the junction width d, the relative feature between the curves $\mathcal{T}(\beta)$ with different E as seen in figure 3 is common for the potentials (9), regardless of the value of d.

Next, in figure 4, we present the current density $I^* = I/W$ (current divided by the sample width) versus the applied bias voltage V ($(I$–$V)$ characteristics) calculated from equation (8) for the three junctions studied in figure 2, setting the zero-bias (equilibrium) Fermi energy to be zero, $\mu_0 = 0$. These I–V curves bear a resemblance to those for the so-called Esaki diode [19], but with a much weaker negative differential resistance (NDR) in the forward-biased part ($V > 0$). Such a smear of NDR in figure 4 is essentially related to the fact that the carriers in graphene are chiral, and therefore both electrons and holes (negative energy electrons) can make a contribution to the current. It seems that just the contribution from negative energy electrons is responsible for the observed reduction of NDR. And, as a matter of fact, the pronounced NDR (and even the hard well in $\mathcal{T}(E)$) claimed in [17][2] for a graphene rectangular barrier is a direct consequence of mistakenly neglecting this contribution. One might assume that such a electron–hole symmetry induced smear of NDR is a common characteristic of graphene nano-structures. Besides, since the forward bias V reduces the difference in potential between two leads (figure 1(b)), in the process of increasing V, at some bias V_c a crossover should occur from the regime where the potential in the p-region, U_R, is higher than that in the n-region, U_L (at $V < V_c$), to the opposite regime with $U_L > U_R$ (at $V > V_c$). This crossover causes a change in sign of the differential transmission $\mathcal{T}$ (not shown) that in turn gives rise to a slight peak in the I–V curves, as can be seen at $V_c = 60$ mV in figure 4. Such a tendency to change the potentials U_R and U_L in forward bias also leads to a reduction of the Klein tunneling region, explaining why the influence of the junction width d on the I–V curve is so weak in applied voltage regime, $V > 0$. On the contrary, in the case of reverse biases ($V < 0$), when the applied voltage enhances the difference in potential between two leads, the Klein tunneling region enlarges with $|V|$, resulting in a considerable reduction of the current magnitude $|I|$ as d increases.

Finally, in figure 5 we show the effective conductance $G^* = G/W$ (the conductance divided by the sample width), calculated from equation (8), as a function of the equilibrium Fermi energy μ_0 for the same junctions as those discussed in figure 4. In all the cases under study, the curve $G(\mu_0)$ is clearly symmetric with respect to the energy $\mu_0 = 0$ (potential origin in the model under study). Understandably, such a symmetry of $G(\mu_0)$ is a consequence of two factors: the symmetry of the potential considered (with respect to the point O in figure 1(b)) and the electron–hole symmetry in graphene. The lead potentials, $U_R = -U_L$, define the energies where G vanishes (−30 and 30 meV in figure 5), while the junction width d affects only the magnitude of G. In the energy range $U_L < \mu_0 < U_R$, when the Klein tunneling is important, G strongly decreases as d increases. Beyond this energy range, while increasing almost linearly with $|\mu_0|$, G experiences only a slight increase with d. The symmetric and linear behavior of the conductance as a function of μ_0 is the typical conduction character of graphene sheets which has

[2] Note that due to mistakenly neglecting contributions from negative energy electrons, the current reported in this work is inaccurate (see Nam Do [17]).

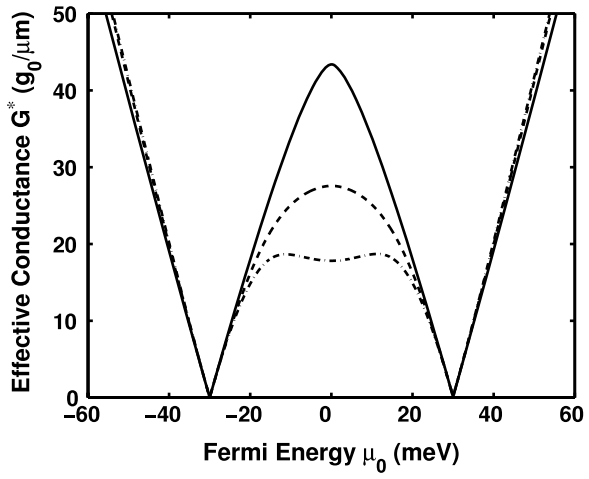

Figure 5. Effective conductance $G^* \equiv G/W$ as a function of the equilibrium Fermi energy μ_0 for the three junctions studied in figure 4 (with the same parameter values and the same meaning for the symbols). The units of G and W are taken here as $g_0 \equiv 2e^2/h$ and μm, respectively.

already been reported in the seminal work [1], where the so-called minimum graphene conductivity was discussed [1, 20].

In conclusion, we have shown that the standard T-matrix method can be used effectively for studying the dynamics of Dirac electrons under 1D-potentials in graphene. To this end, the transmission probability expressed in terms of T-matrices and the corresponding ballistic current have been derived for any smooth 1D-potential, taking into account the chirality of Dirac massless carriers in graphene. As a useful illustration of the suggested approach, numerical calculations have been performed for the potential which approximately describes graphene n–p junctions. Obtained results for the transmission probability as a function of the incident energy as well as the incident angle show the profound effects of the chirality and the Klein tunneling of relativistic carriers in the junction considered. Manifestations of these effects have also been found in the I–V characteristics, which resemble those of Esaki diodes but with much weaker NDR, as well as in the Fermi energy dependence of the conductance, which is symmetric with respect to the potential origin (for the model considered) and very sensitive to the junction width in the range of energy favorable for Klein tunneling. Thus, graphene n–p junctions can be used as an effective tool for examining the dynamical properties of Dirac massless electrons. Finally, it is worth mentioning that the T-matrix approach suggested is quite general and should be applicable to a wide range of graphene nano-structures. In fact, we have performed some calculations of energy structure, conductance and shot noise for some structures such as multiple barriers or n–p–n junctions and the obtained results may be discussed elsewhere.

Acknowledgments

This work was supported by the Ministry of Science and Technology of Vietnam via the Fundamental Research Program (project 4.023.06).

Appendix. Expression for the transmission probability

The chirality is clearly manifested, for example, in the current density expression $\mathbf{j} = v_F \Psi^+ \boldsymbol{\sigma} \Psi$. In the x-direction this expression reduces to $j_x = \mathrm{sgn}(E-U)(2v_F/S)\cos\alpha$, where S is the system area and the angle α is defined as $\cos\alpha = k_x/k \equiv k_x/|E-U|$. So, the relative direction between $\mathbf{j}$ and $\mathbf{k}$ depends on the sign of $(E-U)$. It is worth noting here that the angle α is introduced as a 'quantum number' describing the incoming state in the left lead. It is different from the well addressed incident angle β [4, 8], though there is a simple relation between two angles: $\beta \equiv \alpha$ for positive energies and $\beta = \alpha + \pi$ for negative energies. Such a chiral property of Dirac fermions makes the transmission probability in terms of T-matrices in graphene different from that in semiconductor structures.

Let us calculate the transmission probability $\mathcal{T}(E,\alpha)$ associated with the state (k_x, k_y), or in equivalence (E,α), coming from the left, where $U = U_L$ (figure 1(a)). Taking into account the expression j_x-mentioned above, we notice that $\mathcal{T}$ is non-zero only if $j_x > 0$, requiring either (i) $(E-U_L) > 0$ with $-\pi/2 < \alpha < \pi/2$ or (ii) $(E-U_L) < 0$ with $\pi/2 < \alpha < \pi$ or $-\pi < \alpha < -\pi/2$. The sign of $(E-U_L)$ determines the boundary behaviors for the waves in the left of the active region. Since the transmission probability $\mathcal{T}$ should depend on the boundary behaviors of the waves on both sides of the potential, it should also depend on the sign of $(E-U_R)$ in the right of the active region. In other words, $\mathcal{T}$ should be calculated in four cases corresponding to different signs of $(E-U_R)$ and of $(E-U_L)$ accompanied by the conditions mentioned above for the angle α.

We consider, for example, the case of $(E-U_L) > 0$ and $(E-U_R) > 0$. In the T-matrix equation $(A_N, B_N)^T = T(A_0, B_0)^T$, the first condition, $(E-U_L) > 0$, implies $A_0 = 1$ and $B_0 = r$ (reflection amplitude), while the second condition, $(E-U_R) > 0$, leads to $A_N = t$ (transmission amplitude) and $B_N = 0$. From these boundary amplitudes we readily have $r = -T_{21}/T_{22}$, and therefore $\mathcal{T} = 1 - |r|^2 = 1 - |T_{21}|^2/|T_{22}|^2$, where $T_{ij}(i, j = 1, 2)$ are the T-matrix elements. Note again that in addition to conditions $(E-U_L) > 0$ and $(E-U_R) > 0$ the obtained $\mathcal{T}$ is valid only for $-\pi/2 < \alpha < \pi/2$.

Similarly, we can derive the $\mathcal{T}$-expression in the remaining three cases. Taking into account the condition associated with the angle α, the final result can be written in the form:

$$\mathcal{T} = f(s,\alpha)\begin{cases} 1 - |T_{21}|^2/|T_{22}|^2, \\ \qquad \text{if } (E-U_L) > 0 \text{ and } (E-U_R) > 0 \\ 1 - |T_{11}|^2/|T_{12}|^2, \\ \qquad \text{if } (E-U_L) > 0 \text{ and } (E-U_R) < 0 \\ 1 - |T_{22}|^2/|T_{21}|^2, \\ \qquad \text{if } (E-U_L) < 0 \text{ and } (E-U_R) > 0 \\ 1 - |T_{12}|^2/|T_{11}|^2, \\ \qquad \text{if } (E-U_L) < 0 \text{ and } (E-U_R) < 0. \end{cases} \tag{A.1}$$

Here for compactness the function $f(s,\alpha)$ is introduced to select a correct region of α for each case under study:

$f(s,\alpha) = [(s+1)/2]f_1(\alpha) + [(-s+1)/2]f_2(\alpha)$ where $f_1(\alpha) = \Theta(\pi/2-\alpha)-\Theta(-\pi/2-\alpha)$, $f_2(\alpha) = \Theta(-\pi/2-\alpha)-\Theta(\pi/2-\alpha)-\Theta(-\pi-\alpha)+\Theta(\pi-\alpha)$, $s = 1$ if $(E-U_L) > 0$ and -1 if $(E-U_L) < 0$, and Θ is the standard step function.

We notice that, mathematically, the equalities $T_{21} = T_{12}^*$ and $T_{11} = T_{22}^*$ are strictly realized only in the case when k_x is purely real in both leads. However, physically, we always have $|T_{21}|^2/|T_{22}|^2 = |T_{12}|^2/|T_{11}|^2$ and $|T_{11}|^2/|T_{12}|^2 = |T_{22}|^2/|T_{21}|^2$ that allows us to rewrite (A.1) in the form (6).

References

[1] Novoselov K S, Geim A K, Morozov S V, Jiang D, Katsnelson M I, Grigorieva I V, Dubonos S V and Firsov A M 2005 *Nature* **438** 197

[2] Castro Neto A H, Guinea F, Peres N M R, Novoselov K S and Geim A K 2007 arXiv:0709.1163 [cond-mat.v1]

[3] Beenakker C W J 2007 arXiv:0710.3848 [cond-mat.v1]

[4] Katsnelson M I, Novoselov K S and Geim A K 2006 *Nat. Phys.* **2** 820

[5] DiVincenze D P and Mele E J 1984 *Phys. Rev.* B **29** 1685

[6] Semenoff G W 1984 *Phys. Rev. Lett.* **53** 2449

[7] Silvestrov P G and Efetov K B 2007 *Phys. Rev. Lett.* **98** 016802

[8] Cheianov V V and Fal'ko V I 2006 *Phys. Rev.* B **74** 041403

[9] Pereira J M Jr, Mlinar V, Peeters F M and Vasilopoulos P 2006 *Phys. Rev.* B **74** 045424

[10] Davis J H 1998 *The Physics of Low-Dimensional Semiconductors. An Introduction* (Cambridge: Cambridge University Press)

[11] Datta S 1997 *Electronic Transport in Mesoscopic Systems* (Cambridge: Cambridge University Press)

[12] Brey L and Fertig H A 2006 *Phys. Rev.* B **73** 235411

[13] Calogeracos A and Dombey N 1999 *Contemp. Phys.* **40** 313

[14] Fogler M M, Glazman L I, Novikov D S and Shklovskii B I 2007 arXiv:0710.2150 [cond-mat.v1]

[15] William J R, Dicarlo L and Marcus C M 2007 *Science* **317** 638

[16] Galiskii V M, Karnakov B M and Kagan V I 1981 *Problems in Quantum Mechanics* (Moscow: Nauka) (in Russian) problem 2.51

[17] Dragoman D and Dragoman M 2007 *Appl. Phys. Lett.* **90** 143111
Nam Do V 2008 *Appl. Phys. Lett.* **92** 216101

[18] Jena D, Fang T, Zhang Q and Xing H 2008 arXiv:0806.0139 [cond-mat.mtrl-sci]

[19] Sze S M 1981 *Physics of Semiconductor Devices* 2nd edn (New York: Wiley)

[20] Ziegler K 2006 *Phys. Rev. Lett.* **97** 266802